

FIGURE 2. THE 1.2 M BENT-CASSEGRAIN TELESCOPE LOCATED APPROXIMATELY 70 M FROM THE TRANSMITTER RECEIVED THE DOWNLINKED DATA STREAM. THIS TELESCOPE ALSO MEASURED THE ATMOSPHERIC SEEING WHICH PROVIDED AN ESTIMATE OF THE ATMOSPHERIC TURBULENCE DURING THE TRANSMISSION.

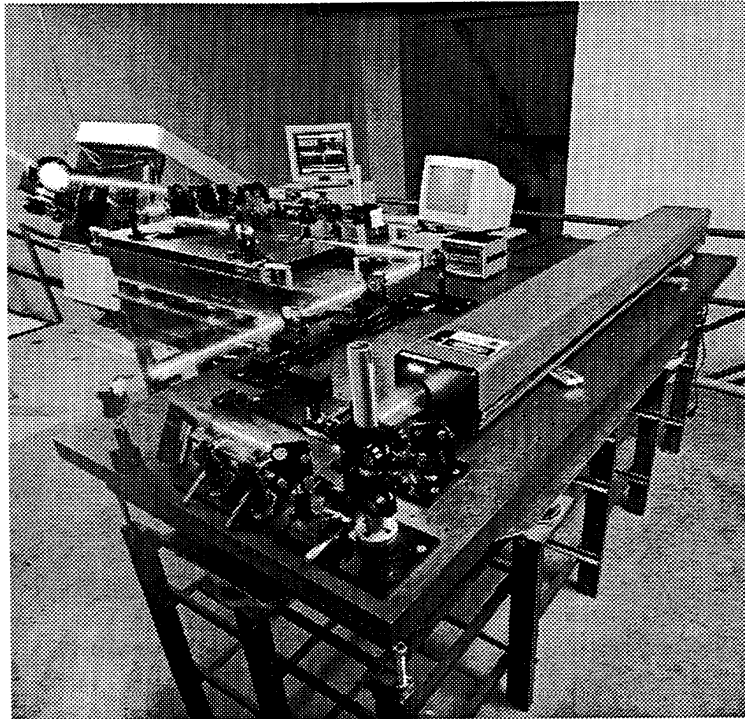


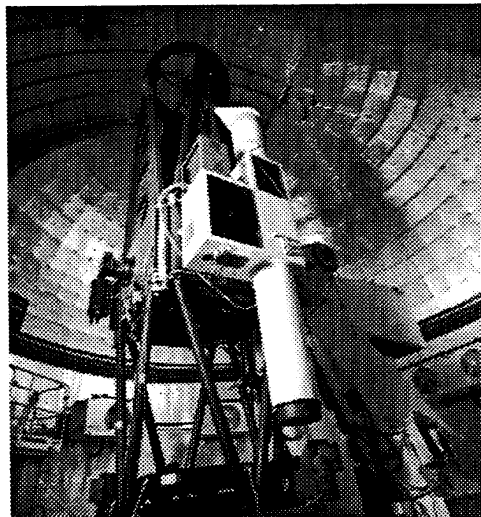
Figure 2 shows the uplink laser in the coude room of the transmitter telescope. It is a 13 W argon-ion laser and it is coupled to the 0.6-m TMF telescope through its coude focus. Theory predicts that transmitting multiple spatially and temporally incoherent beams reduces scintillation and beam wander on the uplink. In the phase-I experiments, we compared single-beam and dual-beam propagation. In the dual-beam experiments, we split the laser output into two spatially and temporally uncorrelated beams of equal intensity and recorded the fluctuation in uplink signal intensity detected at the

satellite. We compared the theoretically predicted and measured variances in the detected intensity fluctuations and found good agreement between theory and experiment (6).

The uplink beam was transmitted in either the data or the beacon modes. In the data mode, the uplink laser was modulated, in the beacon mode it was not. In either mode, however, the uplink served as a reference for pointing the downlink to the ground station. In the data mode, an electro-optic crystal was used to impress a 1.024 Mbps pseudo-random noise (PN) Manchester-coded bit stream on the optical carrier. The uplink beam was demodulated at the satellite and errors in the transmission detected. Although the uplink bit error rates (BERs) varied with atmospheric conditions and uplink pointing accuracy, we were able to measure BERs as low as $1E-4$, under favorable conditions, during the phase-I experiments.

The downlink transmitter was a 30 mW AlGaAs laser coupled to a 7.5 cm onboard refractive telescope. The ground receiver was the 1.2-m telescope shown in Figure 3 that was located approximately 70 m from the transmitter. The satellite has three modes for the optical downlink. These are

FIGURE 3: THE UPLINK LASER WAS PROPAGATED THROUGH A SYSTEM OF OPTICAL RELAY MIRRORS AND LENSES FROM THE TELESCOPE'S COUDÉ ROOM TO THE TRANSMITTER TELESCOPE. AN ELECTRO-OPTIC MODULATOR WAS USED TO IMPRESS THE 1.024 MBPS DATA STREAM ON THE OPTICAL CARRIER.



WIDE-FIELD CCD ASTROMETRIC CAMERA DEVELOPMENT

**TABLE
MOUNTAIN
ASTROMETRIC
CAMERA**



VINCENT POLLMEIER

Shortly after midnight on April 30, 1996, a state-of-the-art, wide-field charge coupled device (CCD) camera system for ground-based astrometry of solar-system bodies and laser-bearing spacecraft, jointly developed by the DSN Technology Program and the Multimission Ground System Office (MGSO) Continuous Improvement Program, was used for the first time at the Table Mountain Observatory Facility. This new camera system uses one of the largest format CCDs currently available. The instrument has a third-of-a-degree field of view and is designed to measure the angular position of a solar-system body at the 0.01-arcsec (approx. 50-nrad) level. This is a factor of 10 improvement over other existing instruments. The camera system was developed to allow the precise determination of ephemerides of natural solar-system bodies including asteroids, comets, and planetary satellites, as well as to provide astrometric position information about future laser-bearing

spacecraft. Observational testing is now underway to verify the camera's performance.

The camera, developed jointly by

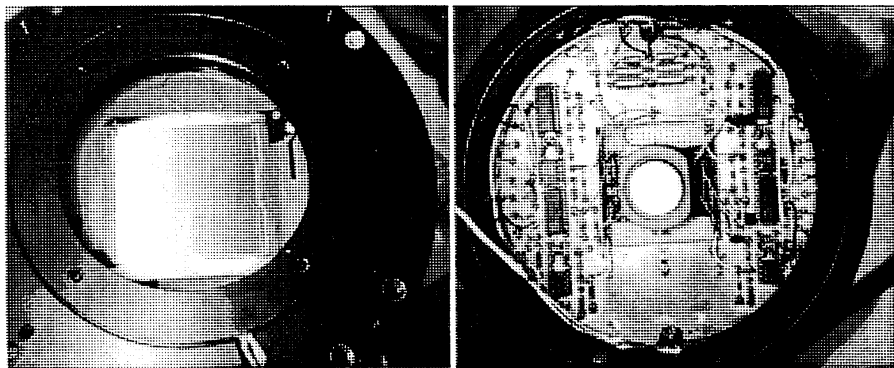


FIGURE 2. CAMERA HEAD SHOWING CCD (LEFT) AND ELECTRONICS (RIGHT) WITH CCD REMOVED (NOTE THE "COLD FINGER" IN THE MIDDLE OF THE HEAD ELECTRONICS).

Divisions 31 and 38, consists of three major portions (shown schematically in Figure 1): the head electronics, the camera mainframe, and a control computer. The head electronics consists of the CCD and the supporting circuitry. The head is directly mounted at the focal point of the telescope and the image is focused on the CCD. The

camera head is shown in Figure 2. The CCD used in this camera contains a 4096×4096 array of 15 micron pixels and measures 6.15 cm on a side. This CCD, manufactured by Loral Corporation, is physically one of the largest CCDs available, based on current manufacturing processes. The CCD is cooled via a

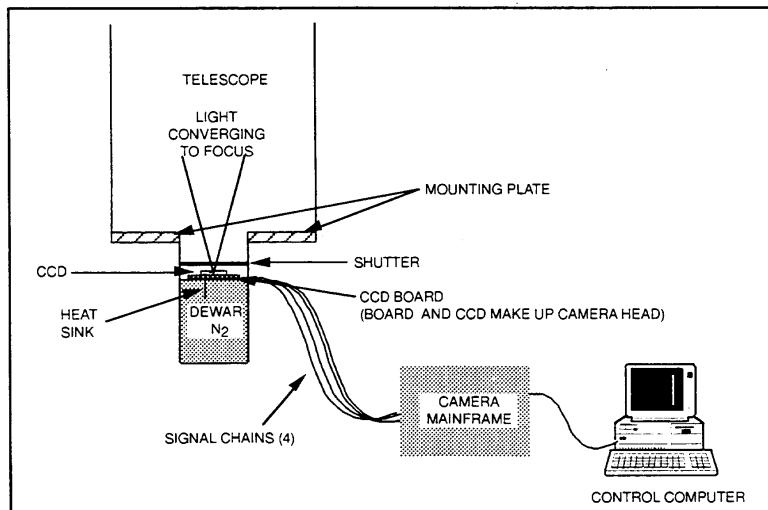
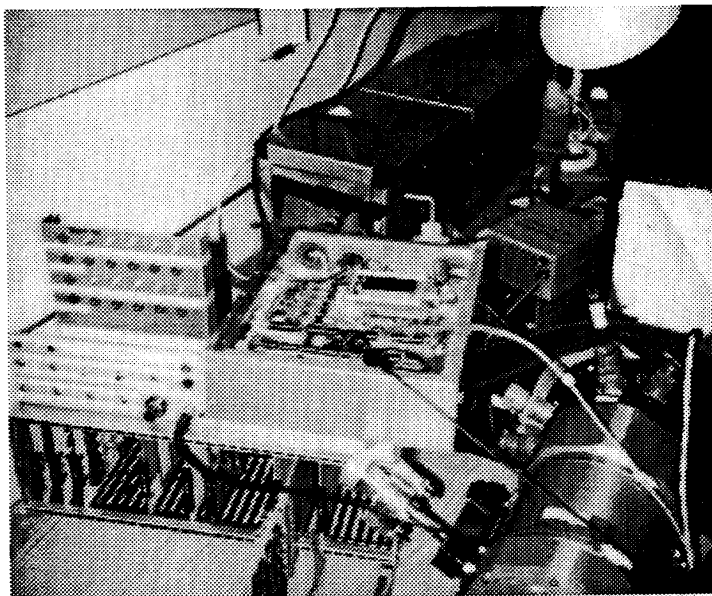


FIGURE 1. SCHEMATIC DIAGRAM OF CAMERA.

CONTINUED ON PAGE 6

FIGURE 3. CAMERA HEAD (NOT VISIBLE) AND MAINFRAME DURING LABORATORY TESTING.



“cold finger” to a liquid nitrogen Dewar. The head is connected to the mainframe by four signal chains, which simultaneously read out the quadrants of the image and assemble them into a single display. The whole system is operated by a PC that controls the electronics and mechanics of the entire camera system (shown in Figure 3 undergoing laboratory testing).

The instrument will make use of the new Hipparcos star catalog. This catalog, from the European Hipparcos mission, will provide positions of stars that are 5 to 10 times more accurate than any other global star catalog. Accounting for degradation of the catalog, due to uncertainties in the

proper motion of the stars, the catalog will retain an accuracy of 0.01 arcsec through the year 2000. However, the average density of the Hipparcos catalog is only 2.4 stars per square degree. Consequently, an instrument that uses this catalog to measure the position of a solar-system body or laser-bearing spacecraft must have a field of view sufficiently wide to mosaic a star field, to acquire a precise measurement. Figure 4 illustrates the process of performing such a measurement. Since in practice it is unlikely that the target of interest will be in the same field of view as an Hipparcos reference star, multiple images will be stitched together by aligning them, using less well-determined stars that appear in the images. However, this mosaic should be as small as possible, as each additional frame that must be stitched together degrades the accuracy of the measurement, and requires the processing of an additional 32 Mbytes of image data. 🐱

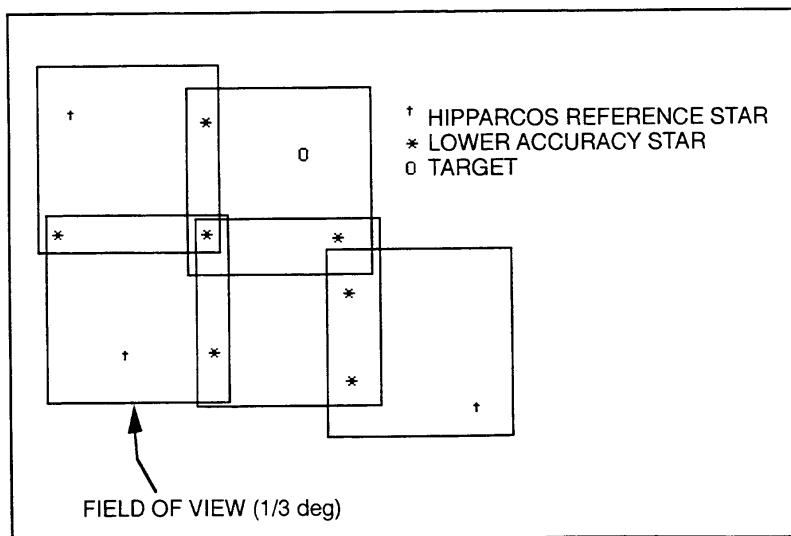


FIGURE 4. MOSAIC SCHEMATIC.